A critical assessment of automatic photoelastic methods for the analysis of edge residual stresses in glass

Augusto Ajovalasit, Giovanni Petrucci and Michele Scafidi

The Journal of Strain Analysis for Engineering Design published online 15 January 2014
DOI: 10.1177/0309324713515466

Review Article

JSA

J Strain Analysis
1–15

DOI: 10.1177/0309324713515466
sdj.sagepub.com
SAGE

A critical assessment of automatic photoelastic methods for the analysis of edge residual stresses in glass

Augusto Ajovalasit, Giovanni Petrucci and Michele Scafidi

Abstract

The measurement of residual stresses is of great importance in the glass industry. The analysis of residual stresses in the glass is usually carried out by photoelastic methods since the glass is a photoelastic material. This article considers the determination of membrane residual stresses of glass plates by digital photoelasticity. In particular, it presents a critical assessment concerning the automated methods based on gray-field polariscope, spectral content analysis, phase shifting, RGB photoelasticity, "test fringes" methods and "tint plate" method. These methods can effectively automate manual methods currently specified in some standards.

Keywords

Glass, residual stress, digital photoelasticity, gray-field polariscope, spectral content analysis, phase shifting, RGB photoelasticity, test fringes, image processing

Date received: 19 July 2013; accepted: 1 November 2013

Introduction

It is well known that photoelasticity is used for the analysis of residual stresses of glass because glass is a photoelastic material.[1,2] The determination of residual stresses in glass, using classical transmission photoelasticity, has been the subject of several contributions, technical standards and commercial equipment based on the use of the following.

- Babinet and Babinet–Soleil compensators[3–6]
- Sénarmont compensation[6–10]
- White light photoelasticity also using the *tint plate*[6,7] and the standard strain discs[1,2,8,9]

The residual stresses in glass plates are given by the superposition of stresses that can be variable with depth (thickness stresses) or constant with depth (membrane stresses). This article concerns the determination of membrane residual stresses in glass plates; for techniques concerning the analysis of thickness stresses in glass plates and for axisymmetric or of any shape components, reference can be made to the literature.[1,11,12]

The development of digital photoelasticity[13–15] allows the user to automate the analysis of residual stresses in the glass. Specifically, the automatic photoelastic analysis of membrane residual stresses was done using the following:

- Gray-field polariscope (GFP)[16–18]
- Spectral content analysis (SCA)[4,19–22]
- Phase-shifting photoelasticity[23–25]
- RGB photoelasticity[25,26]
- *Test fringes* (TF) method[27,28]
- Tint plate method[29,30]

The first two methods require specific equipment, while the remaining methods are based on the use of a classical transmission polariscope interfaced with an image acquisition system. In this article, a critical assessment of the six methods above cited is presented; in particular, for the last four methods, an experimental analysis concerning the determination of the membranal residual stresses in glass plates is also presented.

In this article, the following aspects have been especially considered: availability of commercial systems, restrictions concerning the parameter of the isoclines, acquisition system, additional equipment, system calibration, number of acquisitions and external information needed.

Dipartimento di Ingegneria Chimica, Gestionale, Informatica e Meccanica, Università degli Studi di Palermo, Palermo, Italy

Corresponding author:
Michele Scafidi, Dipartimento di Ingegneria Chimica, Gestionale, Informatica e Meccanica, Università degli Studi di Palermo, Viale delle Scienze, 90128 Palermo, Italy.
Email: michele.scafidi@unipa.it

The photoelastic effect

By photoelastic techniques, the relative retardation δ can be measured. In two-dimensional cases, the retardation δ is related to the principal stresses σ_1 and σ_2 by the well-known equation of photoelasticity

$$\delta = \frac{\Delta}{\lambda} = \frac{C_\lambda d}{\lambda}(\sigma_1 - \sigma_2) \tag{1}$$

where Δ is the absolute retardation, C_λ and d are the photoelastic constant and the thickness of the photoelastic model (glass), respectively, and λ is the wavelength of the monochromatic source. The retardation δ depends on the wavelength λ and on the dispersion of birefringence according to equation (1), which provides

$$\delta = \delta_0 \frac{\lambda_0}{\lambda}\frac{C_\lambda}{C_0} \tag{2}$$

where δ_0 is the retardation at the reference wavelength λ_0 and C_λ/C_0 is the term that takes into account the birefringence dispersion of the used material.[31–33] In monochromatic light with $\lambda = \lambda_0$, equation (2) is reduced to $\delta = \delta_0$.

Near the beveled edge of the glass, the retardation is irregular, and thus, the graphs are usually truncated at the beginning of the bevel; in such a case, the retardation must be extrapolated at the boundary according to well-known procedures as in the case of manual methods.[3,5]

Once the retardation δ_0 is determined, the difference of the principal stresses is evaluated by equation (1) written for the reference wavelength λ_0, which provides

$$\sigma_1 - \sigma_2 = \frac{\lambda_0}{C_0 d}\delta_0 \tag{3}$$

where the photoelastic constant of glasses C_0 usually ranges between 2.4 and 3.6 Brewster (1 Brewster = 1 TPa^{-1}).[34] In this article, the average value $C_0 = 3$ Brewster is assumed.

Especially, the edges of glass sheet are compressed, and due to the boundary conditions, the stress normal to the boundary is $\sigma_y = \sigma_1 = 0$. Thus, the stress σ_x along the boundary is (from equation (3))

$$\sigma_x = \sigma_2 = -\frac{\lambda_0}{C_0 d}\delta_0 \tag{4}$$

The stress normal to the edge (σ_y) is nearly zero even near the boundary, so that equation (4) applies until the zero-order isochromatic fringe, where the inversion of stress from compression to tension happens. Beyond the zero-order fringe, the tensile stress is given again by equation (3)

$$\sigma_x = \sigma_1 = \frac{\lambda_0}{C_0 d}\delta_0 \tag{5}$$

Equation (3) is always valid, while equations (4) and (5) are valid provided that the stress normal to the edge (σ_y) is zero or nearly zero.

GFP

The GFP[16] is shown in Figure 1: it is a circular polariscope in which the quarter-wave plate of the analyzer is eliminated. In this technique, a circularly polarized monochromatic light is incident on the glass and a large number of images are acquired while the analyzer is made to rotate continuously. By properly elaborating the acquired intensities, both the retardation and the isoclinic parameter can be evaluated.

The rotations imposed on the analyzer are

$$\beta_{Ai} = \omega t_i = \frac{\pi}{N}(i-1) \quad i = 1, 2, \ldots, N \tag{6}$$

where ω is the angular velocity of the analyzer, t is the time and N is the number of rotations. N is usually equal to 8, but any $N > 3$ could be used.

The equations of the light intensities acquired for the various positions of the analyzer are

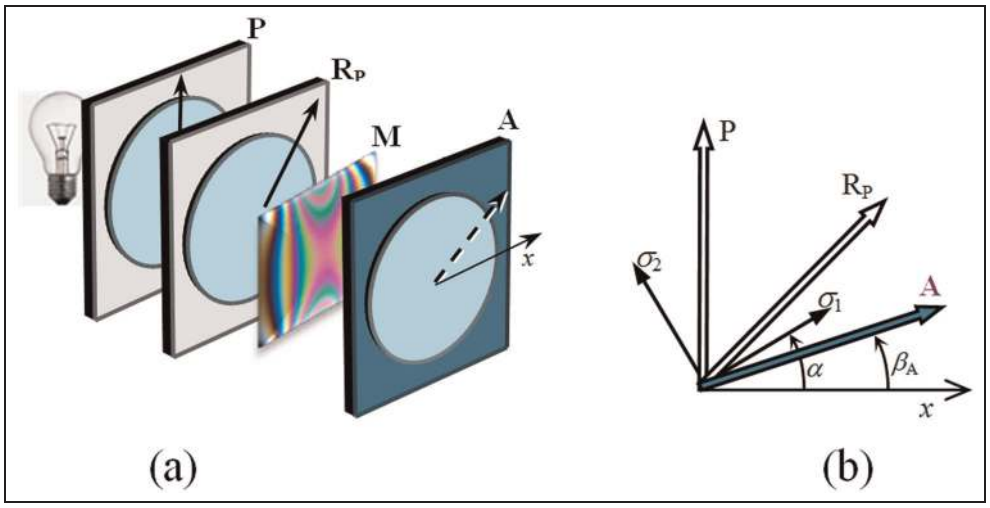

Figure 1. (a) Setup of the polariscope for the GFP method and (b) orientation of principal stresses.

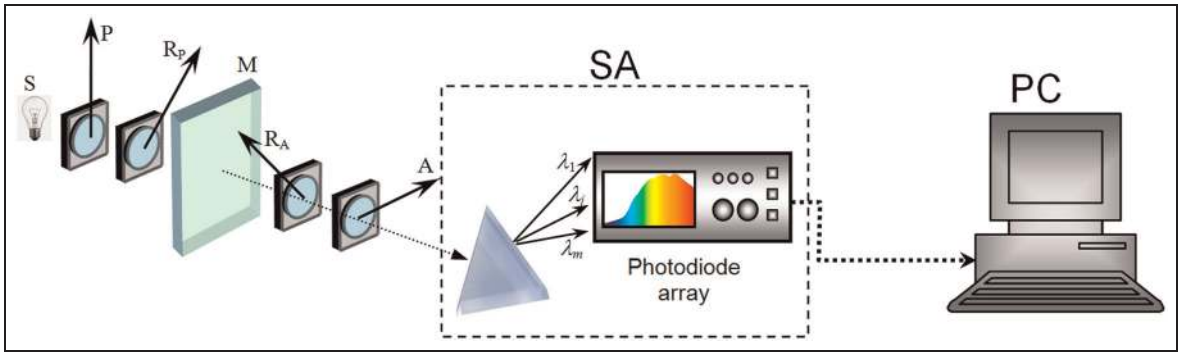

Figure 2. Experimental setup for SCA.
S: light source; P, A: polarizers; R_A, R_P: quarter-wave plates; *M*: model; SA: spectrum analyzer; PC: personal computer.

$$I_i = \frac{1}{2} I_r \left[1 + \sin 2\pi\delta \sin 2(\beta_{Ai} - \alpha)\right] + I_f \tag{7}$$

Using the acquired intensities, the following parameters are first evaluated

$$X = \frac{2}{N}\sum_{i=1}^{N} I_i \sin 2\beta_{Ai} = \frac{1}{2} I_r \sin 2\pi\delta \cos 2\alpha \tag{8}$$

$$Y = \frac{2}{N}\sum_{i=1}^{N} I_i \cos 2\beta_{Ai} = -\frac{1}{2} I_r \sin 2\pi\delta \sin 2\alpha \tag{9}$$

then, the isoclinic parameter can be easily obtained as

$$\alpha = -\frac{1}{2}\tan^{-1}\frac{Y}{X} \tag{10}$$

The retardation can be evaluated by means of the following equation

$$\gamma = \sqrt{X^2 + Y^2} = \frac{1}{2} I_r \sin 2\pi\delta \tag{11}$$

that, for small values of the retardation, leads to

$$2\pi\delta \approx \sin 2\pi\delta = K\gamma \tag{12}$$

where K is a calibration constant that takes into account the system gain and the intensity I_r.

The calibration can be performed by means of a calibration plate of known birefringence δ_0 to be introduced before the analyzer. In particular, the K value can be determined by evaluating the retardation before and after the introduction of the plate and letting their difference equal to δ_0.

SCA

The SCA is based on a spectrophotometer, which determines the spectral content of the light emerging from a circular polariscope using white light. SCA[21] is a point-by-point method although extension toward a full-field method has been proposed.[35] Figure 2 shows a scheme of a typical experimental setup for SCA.

The light emerging from the analyzed point is picked out and conveyed to a prism causing the light to diffract into a spectral band. A photodiode array is then used to detect the light intensities for different bands of wavelength. The resulting light intensity in a dark-field circular polariscope for the generic photodiode i can be written as

$$I_i = I_{fi} + \frac{1}{\lambda_{i2} - \lambda_{i1}} \int_{\lambda_{i1}}^{\lambda_{i2}} I_{0i} \sin^2\left(\pi \frac{\Delta}{\lambda}\frac{C_\lambda}{C_0}\right) \times (1 - \cos^2 2\alpha \sin^2 2\varepsilon) d\lambda \tag{13}$$

where I_{fi} represents the background intensity relative to the generic photodiode i, λ_{i1} and λ_{i2} are the lower and upper boundaries of the spectrum as acquired by a photodiode i, C_λ/C_0 is the term which accounts for the dispersion of birefringence, $\cos^2 2\alpha \sin^2 2\varepsilon$ is the term accounting for the influence of quarter-wave plates which are matched for the reference wavelength λ_0 and ε is the error of the quarter-wave plates.

Equation (13) allows the user to determine the intensity I_i provided that the dispersion of birefringence and the intensities I_{fi} and I_{0i} are known. The intensities I_{fi} and I_{0i} are determined by a calibration procedure. After performing the calibration procedure, the measured intensity I_i^m can be compared to the theoretical intensity I_i^t calculated over a selected range of retardation Δ from equation (13). The unknown retardation corresponds to the value whose theoretical curve best fits the experimental data.

The procedure above mentioned can yield significant errors for low fringe order, in particular lower than 0.5 fringe orders. Methods for enhancing the accuracy of the spectral content method for low levels of retardation were proposed in Ivanova and Nechev[36] and Sanford and McGinnis.[37] These techniques are, in practice, an extension to SCA of the well-known *method of the tint plate* used for quality control of glasses.

The sources of errors of the SCA are due to quarter-wave plates, dispersion of birefringence, bandwidth of the detector and fringe gradient at the point of measurement. The accuracy of the technique was estimated in the order of ± 0.017 fringe orders.[21]

Methods based on classic polariscopes

The four methods described below are based on the use of a classic polariscope interfaced with an acquisition

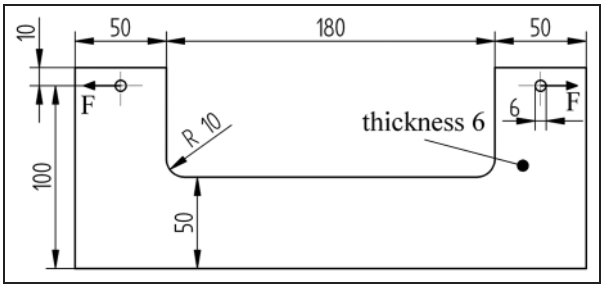

Figure 3. Polycarbonate specimen (dimensions in millimeter) used both as a calibration beam for the RGB method and as carrier for the *test fringes* methods.

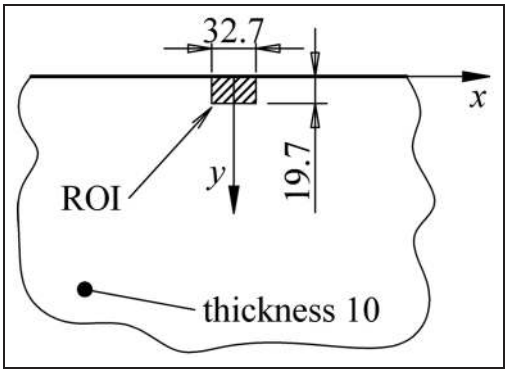

Figure 4. Tempered glass (doors' glass) used in the experiments (dimensions in millimeter).
ROI: region of interest.

system. For these methods, this article also presents an experimental analysis concerning the determination of membranal residual stresses in a glass plate.

Layout and materials

The experiments were carried out using a polariscope with quarter-wave plates matched to the reference wavelength $\lambda_0 = 589$ nm (monochromatic yellow light) using the following.

1. Monochromatic sodium vapor lamps that emit at the reference wavelength ($\lambda_0 = 589$ nm), for the experiments in monochromatic light.
2. Energy-saving fluorescent lamps (Philips Master 7L-D Super 80 18 W/827) with discrete spectral emission having three main narrow band peaks at the following wavelengths: $\lambda_R = 612$ nm (red), $\lambda_G = 546$ nm (green) and $\lambda_B = 436$ nm (blue), for the experiments in white light.
3. An RGB camera, model JVC KY-F30 3CCD, with three independent charge coupled device (CCD) sensors and a Matrox Meteor-2 digital board having a spatial resolution of 768 × 576 pixels and a quantization of 256 RGB levels.
4. A polycarbonate (MM PSM1) specimen (Figure 3), used both as calibration beam and as carrier in the TF methods, and a tempered glass plate (Figure 4), used for the analysis of residual stresses.
5. A full-wave plate (*tint plate*), used in the automated tint plate method (ATPM), having a retardation $\delta_0^c = 1.0$ fringe order at the reference wavelength $\lambda_0 = 589$ nm.

The optical system has been adjusted in order to obtain gradients not higher than 0.1 fringe orders/pixel.[38] The calibration required for the application of the RGB method[38–40] in the TF method was performed using the same specimen (Figure 3) used as a carrier, in which a maximum retardation $\delta_{0max} = 3$ fringe orders was produced.

In the application of the standard RGB method, that is without carrier fringes, and of the ATPM, the so-called self-calibration procedure has been used,[26] as described in the following. In any case, the search of the retardation by the RGB method was carried out by the technique based on the use of a subset of the calibration table.[40]

All the experimental analyses were carried out on a glass door in a region located near the edge, in particular, in the region of interest (ROI) shown in Figure 4. In the ROI, the isoclinic parameter remains almost constant at about 0°. In the comparison among the four methods, the same vertical section in the proximity of the center of the ROI was analyzed. This section has been chosen in the application of the TF method and it coincides with one of the isochromatic fringes of the carrier. In the following, it will be indicated as *reference section*.

Phase-shifting photoelasticity

The phase-shifting method (PSM), introduced in 1986,[41] requires, in the general case, at least four acquisitions. After the pioneering work of Hecker and Morche, based on eight acquisitions, a significant contribution was made by Patterson and Wang,[42] who proposed a method based on the use of circularly polarized light incident on the model and six positions of the analyzer and its quarter-wave plate. The most common general methods are based precisely on six acquisitions. In the application of the PSM, the phase maps of the isoclinic and of the isochromatic fringes are obtained by applying the inverse tangent function to combinations of the light intensities acquired. Due to the periodicity of the tangent function, the phase maps are obtained in wrapped form, so that unwrapping procedures have to be applied in order to evaluate the total retardation.

A method for the unambiguous determination of the retardation and of the isoclinic parameter has been proposed by Aben et al.[24] in the case of retardations of less than half a fringe order. A general review of PSMs is present in Ramesh et al.[15]

In this article, which generally considers retardation higher than 1 fringe order, the general PSM proposed by Barone et al.[43] and the simplified methods[23] have

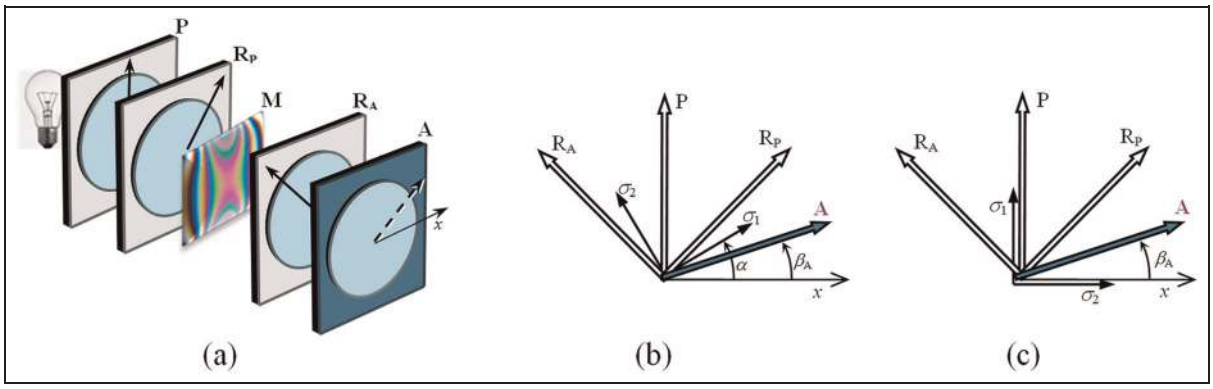

Figure 5. (a) Setup of the polariscope for the Tardy phase-shifting method, (b) general orientation of principal stresses and (c) maximum principal stress σ_1 aligned with the polarizer *P*.

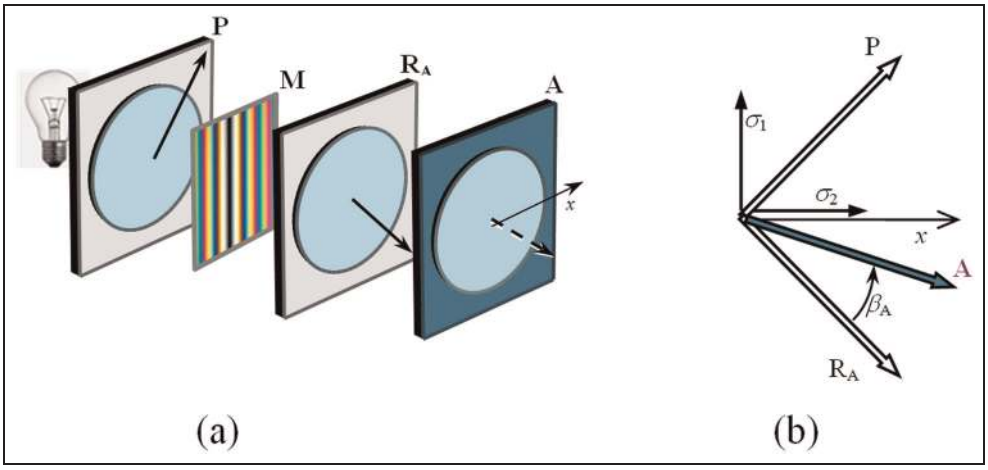

Figure 6. (a) Setup of the polariscope for the Sénarmont phase-shifting method and (b) orientation of the optical elements and the principal stresses.

been used. In particular, the general PSM[43] is based on four acquisitions carried out by using a plane polariscope and two acquisitions using circularly polarized light incident on the model and has the advantage to reduce the effect of the error of the quarter-wave plates, which, if present, is a major cause of inaccuracy of the phase-shifting techniques.[44] In particular, this effect is zero in the determination of the isoclinic parameter and minimum in the evaluation of the retardation when the method of Barone et al.[43] is used.

The simplified methods used in this article are based on the Tardy setup, as initially proposed by Asundi,[45] and on the Sénarmont setup as initially proposed by Ajovalasit et al.[23] In this article, the simplified methods mentioned above, based on the setup of Tardy and Sénarmont, are concisely referred as the Tardy phase-shifting method (TPSM) and the Sénarmont PSM. These simplified PSMs presented in Ajovalasit et al.[23] have the same limitations of the goniometric compensation methods of Tardy and Sénarmont, that is, they need the prior knowledge of the directions of principal stresses. On the other hand, these methods have the advantage that the equation for the evaluation of the retardation does not contain the isoclinic parameter as occurs in the general methods. Due to the fact that at the edges of the glasses the directions of the principal stresses are known (tangent and normal to the boundary), when the residual stress analysis has to be carried out only in their proximity, the simplified methods are preferable.

In Figure 5, a glass plate in the circular polariscope arranged for the Tardy compensation is shown. In Figure 6, the same model is shown in the dark-field polariscope initially arranged for the Sénarmont compensation, with the polarizer P oriented at $+45°$ and the analyzer A with the corresponding quarter-wave plate R_A oriented at $-45°$.

Now, the points of the glass where the principal stresses are directed along the *x*- and *y*-axes (horizontal and vertical) are considered. In particular, assuming that the maximum principal stress σ_1 is directed along the vertical *y*-axis ($\alpha = 90°$, Figures 5(c) and 6(b)), the light intensity emerging from the analyzer for both Tardy and Sénarmont setup is

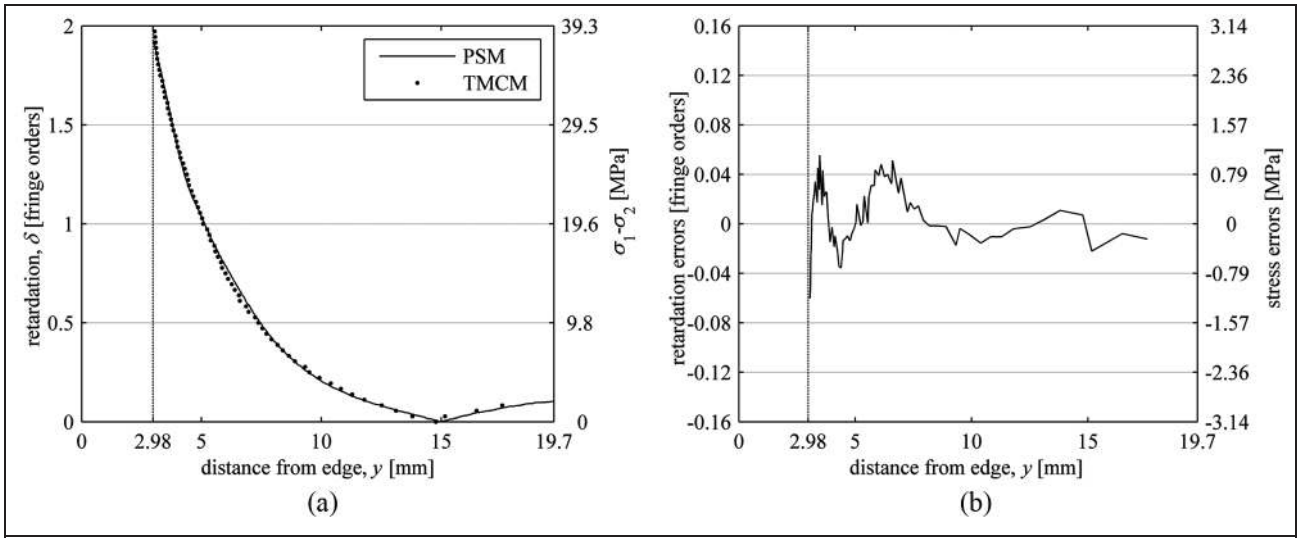

Figure 7. General PSM: (a) retardation δ and principal stress difference ($\sigma_1 - \sigma_2$) along the direction y normal to the edge of the glass at the ROI and (b) errors evaluated with respect to the TMCM.
PSM: phase-shifting method; TMCM: Tardy manual compensation method.

$$I_i = I_f + \frac{I_0}{2}\left[1 - \cos\left(2\pi\delta - 2\beta_{Ai}\right)\right], \quad (i = 1, 2, 3, \ldots) \tag{14}$$

where β_{Ai} is the angle of rotation of the analyzer from its initial position (Figures 5(c) and 6(b)). Equation (14) shows that there are three unknowns (I_f, I_0 and δ), although the unknown of interest is just the retardation δ. Consequently, at least three images with different values of the β_{Ai} angle have to be acquired by properly rotating the analyzer. All the PSM provide only the fractional retardation δ_f which is defined in the range ± 0.5 fringe orders. In order to determine the total retardation δ, unwrapping techniques are used; these techniques require the knowledge of the total retardation δ at least at one point that has to be measured by an independent method.

The effect of the isoclinic error is considered in detail in the literature.[23,46] The positioning of the edge is not critical, as the maximum error on retardation that is about 0.02 fringe orders for isoclinic errors up to about 10° and 20° for Sénarmont and Tardy methods, respectively.

Figure 7(a) shows the results obtained in the reference section with the general PSM. For comparison, the results obtained by the Tardy manual compensation method (TMCM) are shown. Figure 7(b) shows the errors evaluated with respect to the TMCM. The average error is 0.006 fringe orders with a standard deviation (SD) of 0.024 fringe orders.

Figure 8 shows the results obtained by the TPSM, using three acquisitions. For comparison, the results obtained by the TMCM are shown. The average error with respect to the manual compensation method is -0.004 fringe orders with a SD of 0.023 fringe orders.

The results of the PSMs are equivalent to those of TMCM with a significant reduction in the number of acquisitions from about 20–30 for the TMCM to 3–6 in the case of the phase-shifting methods.

RGB photoelasticity

In RGB photoelasticity, the model is placed in a dark-field circular polariscope and the isochromatic fringes are acquired in white light, using a color digital image acquisition system. At each pixel, the three primary colors (red, green and blue) are digitized into three levels of intensity, usually indicated by the symbols R, G and B. Due to the fact that filters of the color cameras are wide-band, the classic equation of the circular polariscope in dark field

$$I = I_0 \sin^2 \pi\delta \tag{15}$$

cannot be used. Not considering the noise and the error of quarter-wave plates, the light intensities captured by the camera are instead expressed by the equation[38,40]

$$I_{wj} = \frac{1}{\lambda_{j2} - \lambda_{j1}} \int_{\lambda_{j1}}^{\lambda_{j2}} I_0(\lambda) T(\lambda) F_j(\lambda) \sin^2\left(\pi\delta_0 \frac{\lambda_0}{\lambda}\frac{C_\lambda}{C_0}\right) d\lambda, \quad (j = R, G, B) \tag{16}$$

where $I_0(\lambda)$ is the light intensity, $T(\lambda)$ is the transmittance that depends on the spectral response of the glass, $F_j(\lambda)$ are the spectral responses of the three camera filters, λ_{j1} and λ_{j2} are the lower and upper limits of the spectral response of the jth filter and the subscript w indicates the use of white light. By means of equation (16), the determination of the retardation δ_0 is not easy, so the method is based on two steps: calibration of the system and search of the retardation. A method for the analysis of stresses in glass artwork, based on the analysis of the RGB colors, is described in Coelho et al.[47]

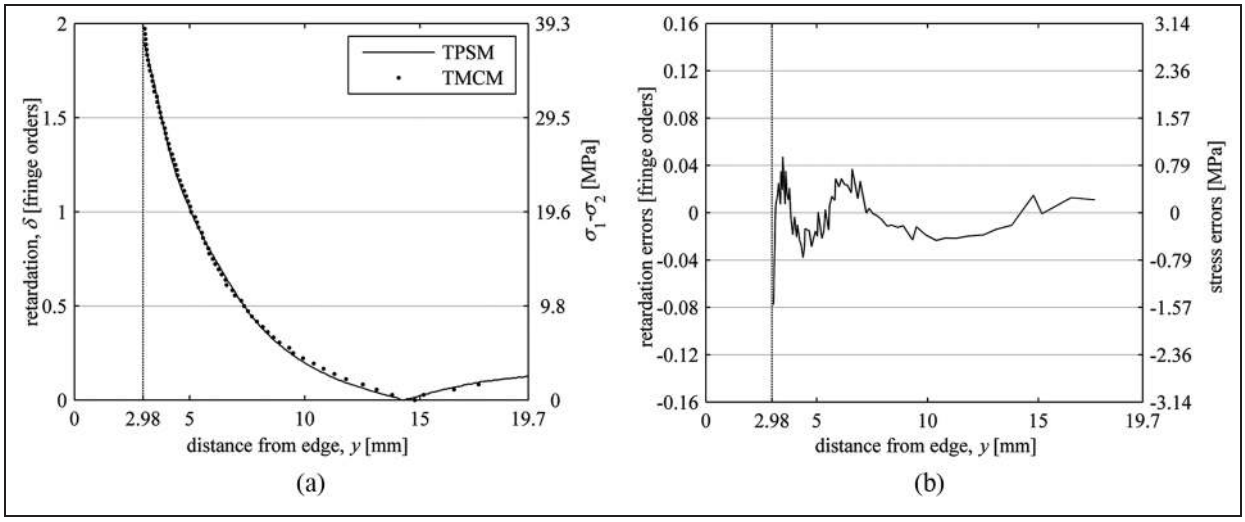

Figure 8. TPSM: (a) retardation δ and principal stress difference ($\sigma_1 - \sigma_2$) along the direction y normal to the edge of the glass at the ROI and (b) errors evaluated with respect to the TMCM.
TPSM: Tardy phase-shifting method; TMCM: Tardy manual compensation method.

Calibration procedure. The usual calibration procedure[38] consists of acquiring the RGB values at each pixel along the transverse symmetry section of a calibration specimen subjected to bending. Each R_i, G_i and B_i triplet is stored in a calibration table or look-up table (LUT) and is associated with a retardation value δ_{0i}. In general, the material of the calibration specimen must match the material used in the test. Otherwise, it is necessary to take into account both the different spectrum of colors and the different dispersion of birefringence.

Since the realization of a glass calibration specimen in bending is not simple in some instances, an alternative self-calibration procedure, defined briefly as Self-Cal, has been proposed by Ajovalasit et al.[26] The Self-Cal procedure consists in creating the LUT using a glass equal to that to be analyzed, subjected to residual stresses not lower than those to be measured. As an alternative to the Self-Cal, it is possible to use a specimen of different material and to apply a color adaptation technique,[48] as long as the effect of the different dispersion of the birefringence relative to the glass plate and the calibration beam is negligible.[26]

Search for retardation. In the search procedure, the R, G and B levels at points, where the retardation is unknown, are acquired. Each R, G and B triplet is then compared with the triplets R_i, G_i and B_i stored in the calibration table by means of an error function defined as

$$e_i = \sqrt{(R_i - R)^2 + (G_i - G)^2 + (B_i - B)^2} \qquad (17)$$

In each pixel, the index i that minimizes the error function (17) is determined and the retardation is calculated by the relationship

$$\delta_{0i} = \delta_{0N} \frac{i}{N}; \quad 0 \leqslant i \leqslant N \qquad (18)$$

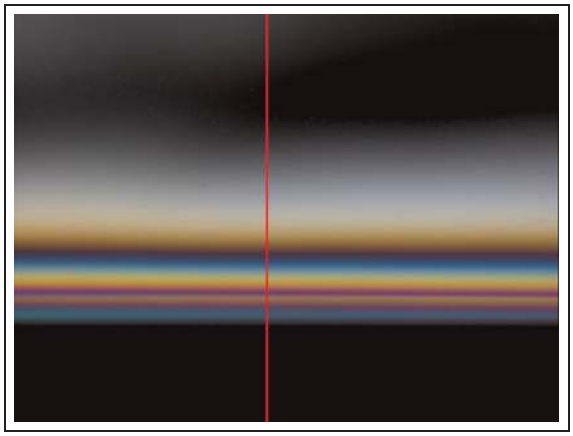

Figure 9. Isochromatic fringes in dark field at the ROI of the doors' glass and the measurement section (—) (color figure in the online version of this article).

where, as previously mentioned, δ_{0N} is the maximum retardation of the calibration table and N is the index of the last element in the calibration table.

The described procedure can be applied by evaluating the error function (17) for all the elements of the LUT ($i = 0, 1, \ldots, N$), or for a subset of it.[40,49] A procedure that uses the second option, which implicitly contains the condition of continuity of the retardation, reduces the computational time and the errors. In particular, the reduction in the errors is similar to that of procedures explicitly using the condition of continuity of the retardation.[50,51]

Experimental results. Figure 9 shows the isochromatic fringes at the ROI and the reference section chosen for the measurement of the retardation. Figure 10(a) shows the retardation δ_0 and the principal stress difference ($\sigma_1 - \sigma_2$) along the measurement section determined by

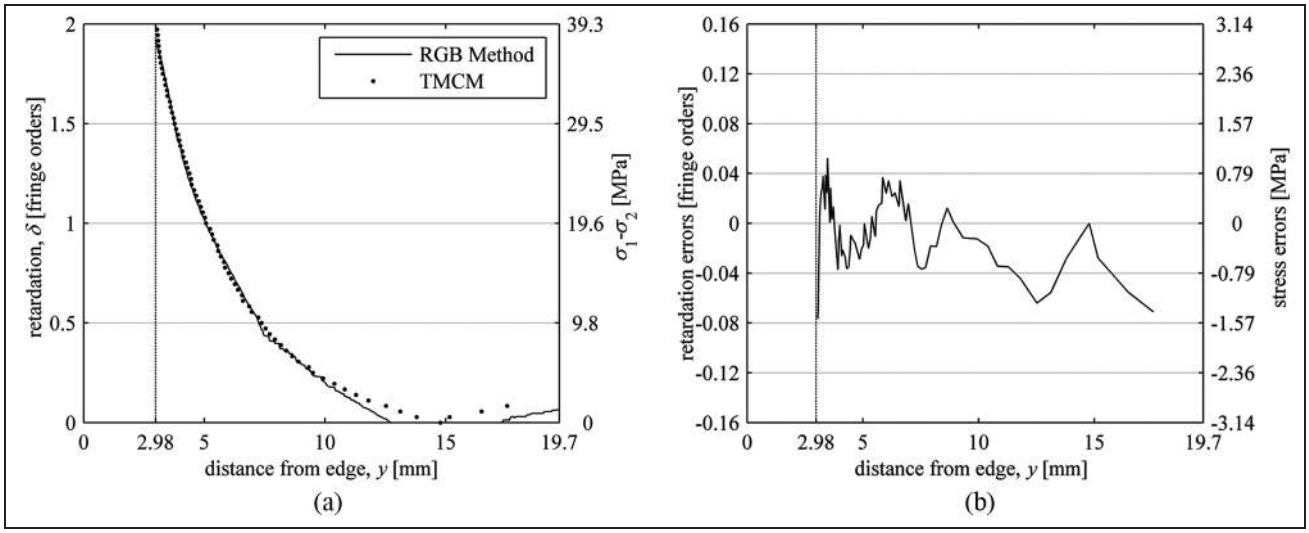

Figure 10. RGB photoelasticity: (a) retardation δ and principal stress difference ($\sigma_1 - \sigma_2$) along the direction y normal to the edge of the glass at the ROI and (b) errors evaluated with respect to the TMCM.
TMCM: Tardy manual compensation method.

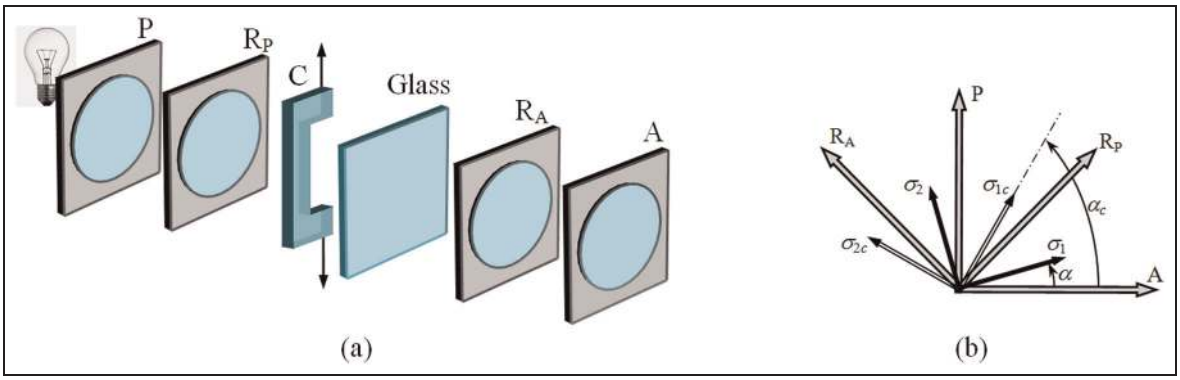

Figure 11. Test fringes method: (a) polariscope and (b) orientation of the optical elements.
C: carrier; P, A: polarizers; R_P, R_A: quarter-wave plates; σ_1, σ_2: glass principal stresses; σ_{1c}, σ_{2c}: carrier principal stresses; α, α_c: orientation of principal stresses in the glass and the carrier.

the RGB method and, for comparison, by the TMCM. Figure 10(b) shows the error with respect to the TMCM. The average error is -0.009 fringe orders with a SD of 0.028 fringe orders. It is possible to see that the highest errors (higher than -0.04 fringe order) occur in the field $0 \leqslant \delta \leqslant 0.5$ fringe orders, in which the colors of isochromatic fringes degenerate into gray tones. In this case, at each pixel, the three R_i, G_i and B_i levels assume similar values, and the RGB method is not able to eliminate the influence of the possible fluctuation of the reference light field and of electronic noise, as also reported in Ajovalasit et al.[38]

TF methods

In the photoelastic analysis of residual stresses in glass, it is common practice to insert (Figure 11) behind or ahead the glass a Babinet compensator or even a simple specimen subjected to bending, in order to obtain a system of reference fringes (isochromatics) parallel and having the same pitch p. The carrier is placed with the axis orthogonal to the edge of the glass so as to obtain near the edge itself one of the two conditions $\alpha - \alpha_c = 0°$ or $\alpha - \alpha_c = \pm 90°$.

The resulting fringes, which are sometimes called TF,[1] effectively reveal the presence of residual stresses. As an example, Figure 12 shows the isochromatic fringes in the bent specimen alone (below) and into the glass superimposed on the specimen subjected to bending (above).

In general, another effect of the reference fringes is that the retardation into the glass plate is increased. This is a positive effect because it produces an increment in the retardation in areas near the fringe of zero order, where the retardation is too low to be measured accurately using the RGB methods.

Analysis in monochromatic light by the center fringe method. In this case, methods based on the extraction of the center of the fringes,[13] which for brevity are

designated as center fringe methods (CFMs), are used. The analysis in monochromatic light by the CFM is applicable near straight edges with isochromatic fringes parallel to the edge and reference fringes orthogonal to the edge.[28] This method has also been recovered in Naveen et al.[52] where the effect of the carrier fringe density is considered.

With reference to Figure 12, considering the line passing through the center of a carrier fringe of order i (retardation δ_i^c, abscissa x_i), the retardation δ at a point of the glass plate along the same line is directly proportional to the distance $x-x_i$ between the point itself and the isochromatic fringe of the same order i (retardation $\delta^{tot} = \delta_i^c$, abscissa x) present in the glass.[27,28]

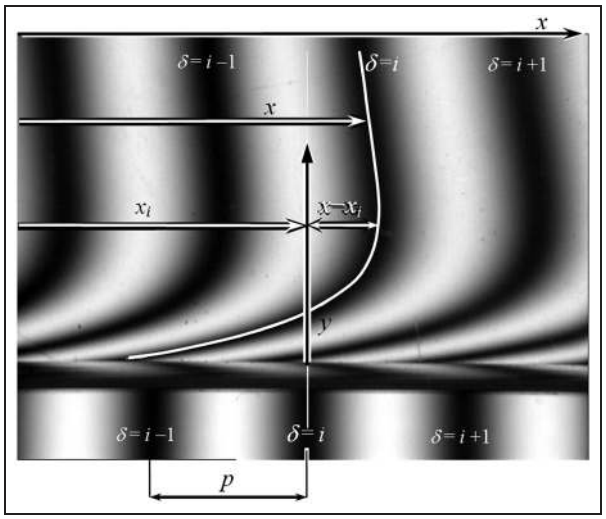

Figure 12. Isochromatic fringes (above) in the glass superimposed on the carrier (*test fringes*) and in the carrier alone (below). The parameters for the CFM evaluation are also indicated.

In this case, in order to obtain the retardation along a vertical section, it suffices to determine the location of the centers of an isochromatic in the glass and the position of the straight isochromatic fringe of the same order in the carrier. The retardation is given by Ajovalasit et al.[28]

$$\delta_{CF} = \frac{|x - x_i|}{p} \tag{19}$$

Figure 13(a) shows the retardation δ_{CF}, given by equation (19), along the measuring section and, for comparison, the results obtained by the TMCM. In the same figure, the principal stress difference $(\sigma_1-\sigma_2)$ is also shown. Figure 13(b) shows the error with respect to the TMCM. The average error is 0.004 fringe orders with a SD of 0.019 fringe orders.

Analysis in white light by RGB photoelasticity. The analysis in white light by RGB photoelasticity (TF-RGB) is applicable near straight edges with reference fringes orthogonal to the edge. As previously mentioned, the use of reference fringes generally produces an increase in the retardation that has a positive effect on the accuracy of the methods in white light, which may be subject to large errors for low levels of retardation, as occurs for the RGB photoelasticity.[38]

In the application of the RGB technique, the same polycarbonate specimen shown in Figure 3 was used to perform the calibration and to produce the reference fringes. When the specimen is superimposed on the glass plate, the following retardations are determined.

1. The total retardation in the glass plate superimposed on the carrier δ_0^{tot}.
2. The retardation δ_0^c in carrier alone.

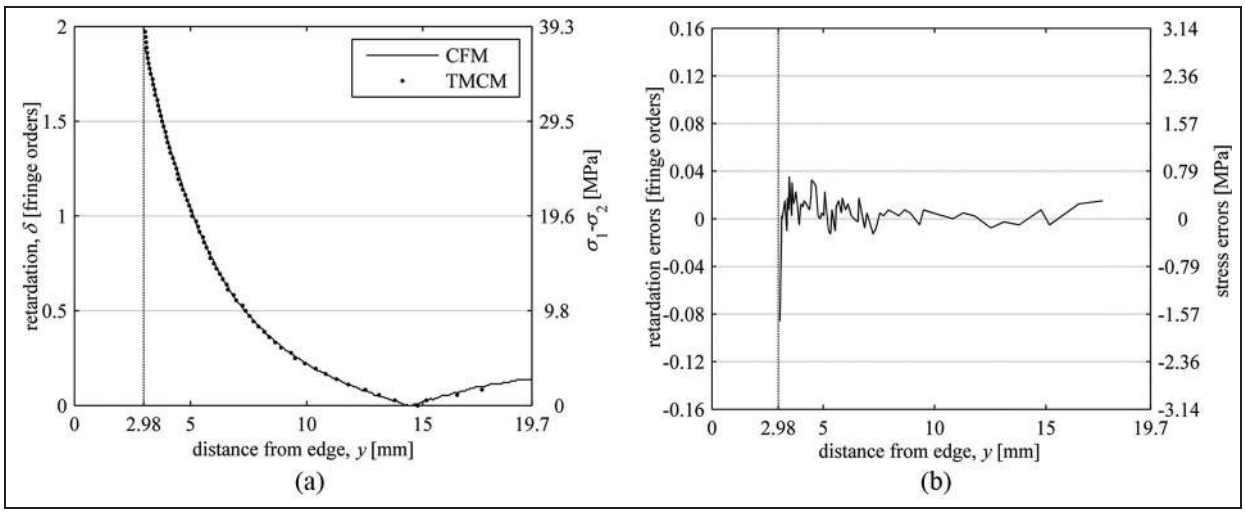

Figure 13. Test fringes method with CFM: (a) retardation δ_{CF} and principal stress difference $(\sigma_1-\sigma_2)$ along the direction y normal to the edge of the glass at the ROI and (b) errors evaluated with respect to the TMCM.
CFM: center fringe method; TMCM: Tardy manual compensation method.

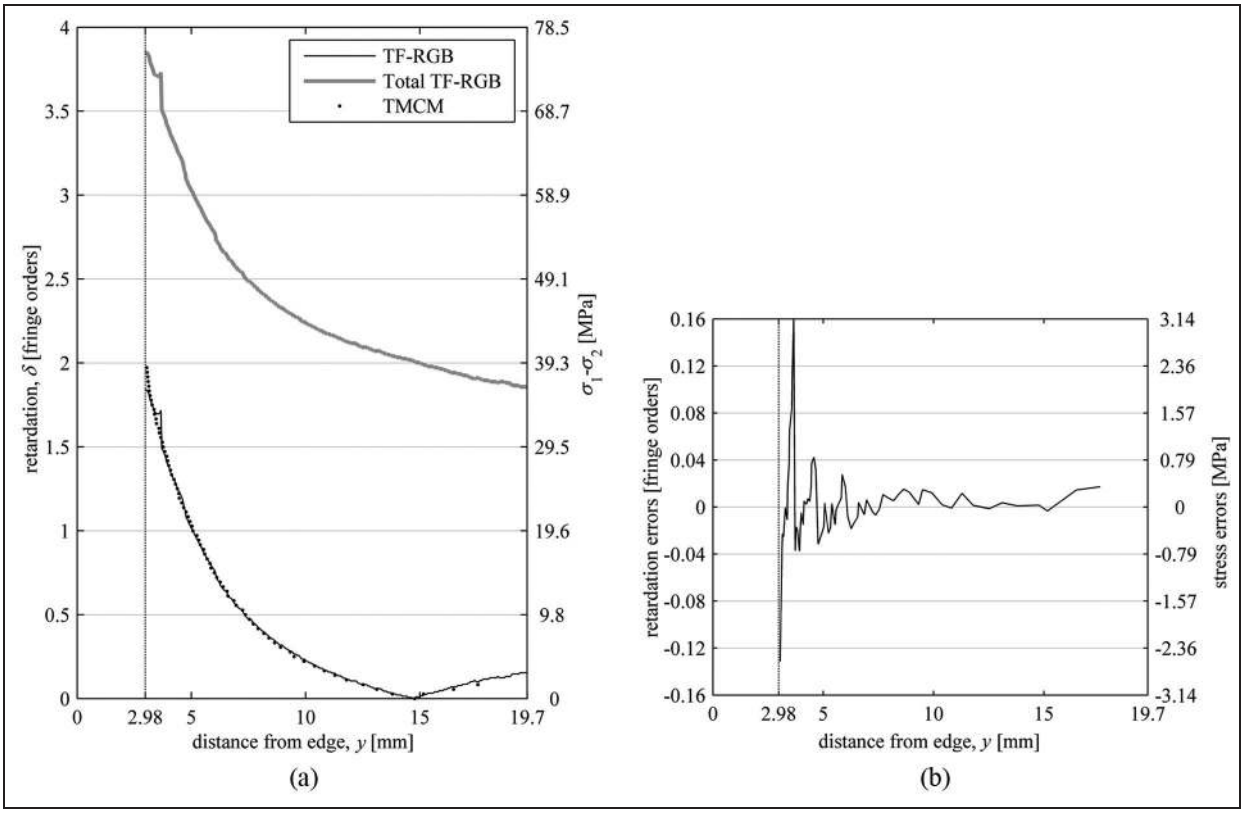

Figure 14. *Test fringes* method with RGB photoelasticity (TF-RGB): (a) retardation δ_0, total retardation δ_0^{tot} and principal stress difference ($\sigma_1-\sigma_2$) as a function of the distance from the edge of the glass and (b) errors evaluated with respect to the TMCM. TF: test fringes; TMCM: Tardy manual compensation method.

From δ_0^{tot} and δ_0^c, the retardation δ_0 in the glass is obtained using the following equation[28] valid (see Figure 11) for $\alpha-\alpha_c = 0°$ and for $\alpha-\alpha_c = \pm 90°$ with $\delta^c > \delta$ (the usual cases)

$$\delta_0 = \left|\delta_0^{tot} - \delta_0^c\right| \tag{20}$$

In the application of this method, the reference section of the glass door lied at the abscissa of the second-order fringe in the tensile side of the carrier. In this section, the conditions of validity of equation (20) are verified. Figure 14(a) shows the total retardation δ_0^{tot} and the retardation δ_0 in the glass determined by equation (20), where, obviously, $\delta_0^c = 2.0$ fringe orders. In the same figure, the results obtained by the TMCM and the principal stress difference ($\sigma_1-\sigma_2$) are also shown. Figure 14(b) shows the error e with respect to the TMCM. The average error is -0.0003 fringe orders with a SD of 0.039 fringe orders.

ATPM

The technique consists in inserting in series with the glass specimen a full-wave plate, usually called *tint plate*, with the optical axes aligned with the directions of the glass principal stresses so as to introduce a constant retardation which is added algebraically with the retardation in the glass. The polariscope is the same as that shown in Figure 11 where the tint plate is inserted in place of the carrier C. The use of the tint plate is particularly useful near the fringe of 0th order where the retardation is low and significant measurement errors could be committed when RGB photoelasticity is used, as it is well known.[38] The use of RGB photoelasticity, jointly to the tint plate, initially proposed in a qualitative way,[29] has been further developed in Ajovalasit et al.[30]

Calibration. As already mentioned, the Self-Cal procedure was used, but in this application, the tint plate has to be placed in series with the glass in both the calibration and search phases. In this case, in the LUT, each set of R_i, G_i and B_i values is associated with the total retardation $\delta_{0i}^{tot} = \left|\delta_0^c \pm \delta_{0i}\right|$.

Search for retardation. In the measuring step, the R, G and B levels at the points where the retardation is unknown are acquired, always using the tint plate. Each set of R, G and B levels is then compared with the R_i, G_i and B_i levels stored in the LUT. The unknown retardation $\delta_0^{tot} = \left|\delta_0^c \pm \delta_0\right|$, at the reference wavelength λ_0, is the one corresponding to the values R_i, G_i and B_i that minimize the error function (17). To this end, in each pixel, the index i of the element of the calibration

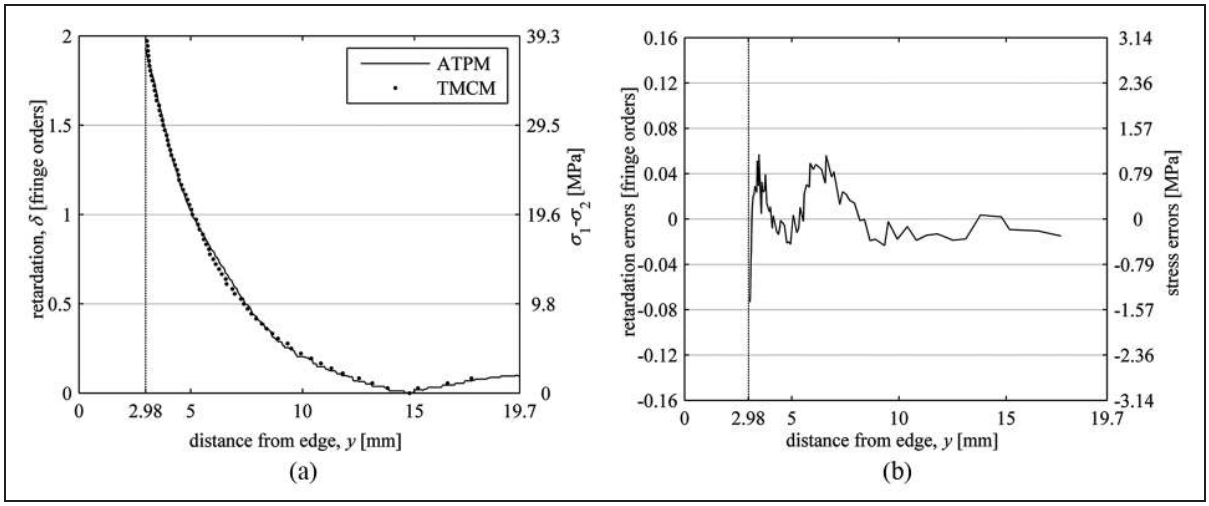

Figure 15. ATPM: (a) retardation and principal stress difference ($\sigma_1 - \sigma_2$) as a function of the distance from the edge of the glass y and (b) errors evaluated with respect to the TMCM.
ATPM: automated tint plate method; TMCM: Tardy manual compensation method.

table that minimizes the error function (17) is determined. The retardation is computed using the relationship[30]

$$\delta_{0i}^{tot} = (\delta_{0N}^{tot} - \delta_{00}^{tot})\frac{i}{N} + \delta_{00}^{tot}; \quad 0 \leqslant i \leqslant N \tag{21}$$

where δ_{0N}^{tot} is the maximum retardation of the calibration table and N is the index of the last element of the calibration table (corresponding to δ_{0N}^{tot}). δ_{00}^{tot} is the minimum retardation of the calibration table corresponding to the first element of index $i = 0$ (NB: usually, the analysis starts from the fringe of order 0 and then $\delta_{00}^{tot} = 0$).

Once the total retardation δ_0^{tot} is determined by RGB photoelasticity and the retardation δ_0^c of the tint plate is known, the retardation in the glass can be obtained simply using equation (20) valid, as already said, in the usual cases of $\alpha - \alpha_c = 0°$ and $\alpha - \alpha_c = \pm 90°$ with $\delta^c > \delta$.

Experimental results. Also, in this case, the experimental results refer to the reference section of the ROI (see Figure 9). Figure 15(a) shows the retardation and the principal stresses difference ($\sigma_1 - \sigma_2$) determined by the ATPM and, for comparison, by the TMCM.

Figure 15(b) shows the errors compared to the TMCM. In particular, the average error is 0.006 fringe orders with a SD of 0.026 fringe orders.

The effect of the incorrect positioning of the tint plate optical axes with respect to the stress directions is experimentally analyzed by Ajovalasit et al.[30] Such analysis shows that the misalignment is not critical.

Figure 16(a) shows the direct comparison between the ATPM, the RGB method and the TF-RGB method in the zone of the measurement section with retardation not higher than half fringe order. The retardation evaluated by the TMCM and the principal stress difference are also shown. Figure 16(b) shows the errors of the three methods evaluated with respect to the TMCM.

Figure 16 clearly shows that the RGB method by itself is affected by not negligible errors in the field $\delta < 0.5$ fringe orders and that such errors can be reduced using the tint plate (TF-RGB) or the reference fringes (TF-RGB).

The average errors are -0.027 fringe orders, 0.006 fringe orders and -0.006 fringe orders for RGB method, TF-RGB method and ATPM, respectively, with a SD of 0.022 fringe orders for RGB method, 0.007 fringe orders for the TF-RGB method and 0.014 fringe orders for the ATPM.

Stresses

The stress σ_x along the y-direction normal to the edge glass was evaluated using equations (4) and (5). As mentioned above, these equations are valid near the edge where the edge orthogonal stress σ_y is nearly zero. For the tested glass, the value of the photoelastic constant $C_0 = 3$ Brewster was used.

Figure 17 shows the σ_x stress in the reference section of the ROI in the glass door, determined by the simplified PSM TPSM (from Figure 8) and, for comparison, by the TMCM, as a function of the distance from the edge. The results obtained using the other methods are practically equivalent.

Discussion and conclusion

This article concerns a critical assessment of the following automated methods of analysis of edge residual stresses in glass: GFP, SCA, general and simplified method of phase shifting, RGB photoelasticity by self-calibration procedure, TF methods, using the CFM in monochromatic light and RGB photoelasticity in white light, and finally the ATPM. The methods analyzed in the article can effectively automate manual methods, many of which are reported by technical standards.

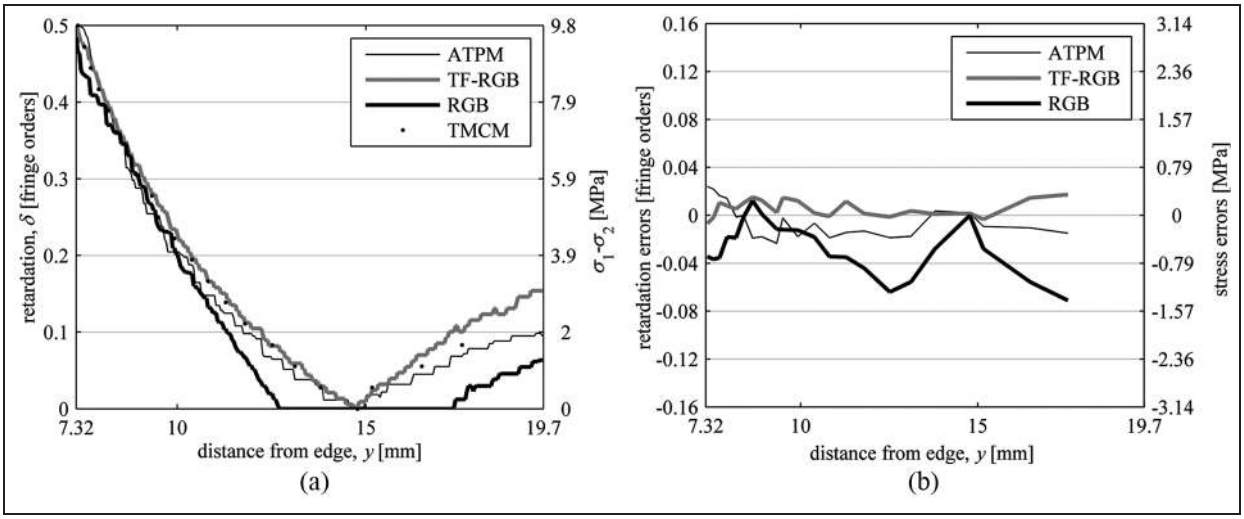

Figure 16. Comparison between the ATPM, the TF-RGB method, the RGB method and the TMCM for low retardations ($\delta \leqslant 0.5$ fringe orders): (a) retardations and principal stress differences ($\sigma_1 - \sigma_2$) as functions of the distance y from the edge of the glass and (b) errors evaluated with respect to the TMCM.
ATPM: automated tint plate method; TF: test fringes; TMCM: Tardy manual compensation method.

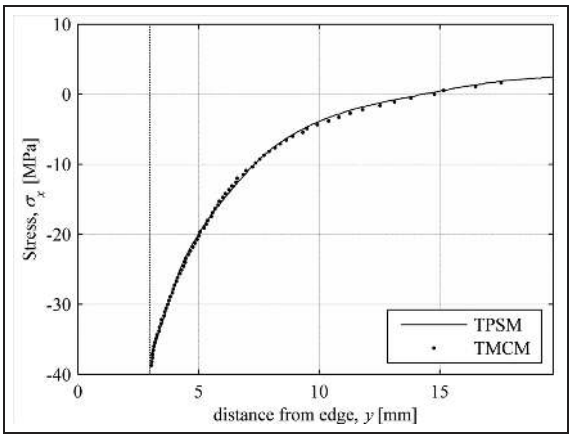

Figure 17. Stress σ_x along the measurement section of the ROI based on the simplified phase-shifting method TPSM and the manual compensation method TMCM.
TPSM: Tardy phase-shifting method; TMCM: Tardy manual compensation method.

Table 1 shows indicatively the correspondence between the manual and automatic methods indicated above.

Table 2 summarizes the characteristics of the methods described above with reference to the following aspects: (1) commercial apparatus, (2) restrictions on the parameter of the isoclines, (3) acquisition system, (4) additional equipment, (5) system calibration, (6) number of acquisitions and (7) external information. These aspects are discussed below.

Commercial apparatus

Commercial devices for the analysis of membranal residual stresses in the glass have been proposed in the market[4,10,12,18] such as the Edge Stress Meter marketed by Sharples[10] based on the compensation of Sénarmont, the GF 1200 polariscope sold by Glass Photonics[18] based on GFP, the automated edge-stress measurement system PES-100 marketed by Strainoptic Technologies[4] based on SCA and the automated polariscope AP-06 proposed by GlasStress[12] based on the general PSM. The other methods, as well as the general PSM, can be easily implemented using components normally found in photoelastic laboratories.

Restrictions on the parameter of the isoclines

The limitation regarding the isoclinic parameter applies to all methods except GFP and SCA methods and the PSM and RGB photoelasticity. The other methods can

Table 1. Correspondence between manual and automatic photoelastic methods for analysis of residual stress in glass.

Manual methods	References	Automatic methods
Goniometric compensation	ASTM C978,[6] ASTM F218,[7] ASTM C148[8] and UNI 7220:1997[9]	Phase-shifting methods, GFP
White light photoelasticity	ASTM C978,[6] ASTM F218,[7] ASTM C148[8] and UNI 7220:1997[9]	RGB photoelasticity, SCA
White light photoelasticity with tint plate	ASTM C978[6] and ASTM F218[7]	Automated tint plate method, SCA
Test fringes method	Aben and Guillemet[1]	Automated *test fringes* methods:
Babinet and Babinet–Soleil compensators	ASTM 1279[5] and ASTM C978[6]	CFM and RGB methods

GFP: gray-field polariscope; SCA: spectral content analysis; CFM: center fringe method.

Table 2. Characteristics of photoelastic methods for analysis of membrane residual stresses in glass.

Method	Commercial apparatus	Isoclinic limitation	Acquisition system	Additional equipment	System calibration	Number of acquisitions	External information
Goniometric compensation (TMCM)	Yes	Yes	–	–	–	20–30	Yes
GFP	Yes	No	Monochrome	Special equipment	Yes	8–16	No[a]
SCA	Yes	No	Monochrome	Special equipment	Yes	Point by point	No
Phase shifting (general), PSM	Yes	No	Monochrome	No	No	4–6	Yes
Phase shifting (simplified), TPSM	No	Yes[b]	Monochrome	No	No	3	Yes
RGB photoelasticity	No	No	Color	No	Yes	1	No
TF by CFM	No	Yes[c]	Monochrome	Yes[d]	No	1	No
TF by TF-RGB	No	Yes[e]	Color	Yes[d]	Yes	1	No
ATPM	No	Yes[f]	Color	Yes[g]	Yes	1	No

TMCM: Tardy manual compensation method; GFP: gray-field polariscope; SCA: spectral content analysis; CFM: center fringe method; PSM: phase-shifting method; TPSM: Tardy phase-shifting method; TF: test fringes.
[a]For small values of the retardation.[b]Applicable near straight or slightly curved edges.[c]Applicable near straight edges, with isochromatics parallel to the edge and reference fringes orthogonal to the edge.[d]Babinet compensator or specimen subjected to bending. [e]Applicable near straight edges with reference fringes orthogonal to the edge. [f]Applicable near straight edges with tint plate axes properly aligned to the edge. [g]Tint plate or specimen subjected to tension (or Babinet–Soleil compensator).

be used for the determination of residual stresses close to straight edges where the isoclinic parameter is known and constant. The misalignment of the isoclinic parameter is not critical: thus, isoclinic errors up to about 10°, 15° and 20° are permissible for the Sénarmont PSM, ATPM and TPSM, respectively.

Acquisition system

The methods based on the SCA technique and RGB photoelasticity require the use of a color image acquisition system, while for all the other techniques a monochromatic system is used.

Additional equipment

The additional equipment (carrier), consisting of a Babinet compensator or a bending specimen, is required by TF methods in order to modulate the fringes in the glass. A full-wave plate is required for the ATPM. The GFP and SCA methods require special equipments.

System calibration

Calibration of the system is necessary for methods that use GFP, SCA and RGB photoelasticity.

Number of acquisitions

The number of acquisitions, which is up to 20–30 for manual goniometric compensation methods and between 4 and 6 (usually 6) for the general method of phase shifting, is 3 for the simplified PSMs and 1 for the others. The GFP requires the rapid acquisition of 8 or 16 images that are obtained rotating the analyzer by a dedicated automated system.[18] The SCA is a point-by-point method although the acquisition is very rapid.[4]

External information

PSMs require external information (the total retardation at a point of the model) in order to correctly identify the fringe order after the unwrapping procedure. The GFP does not require an external information (in the case in which the retardation is low enough to consider equation (12) as true).

In the following, some considerations on the use of the proposed methods are indicated, based on the data presented in Table 2. Methods such as GFP and SCA are well established as evidenced by the commercial equipment available. For the characteristics and performance of these devices, reference is made to information provided by the manufacturers.[4,18] For what concerns the methods based on traditional polariscopes, and therefore implementable without resorting to special equipment, the considerations given below can be made.

As a general rule, the PSMs and, in particular, the simplified ones are preferable. In fact, these methods do not require calibration procedures and carrier fringes. Moreover, the relative low retardation reduces the difficulties in the application of the unwrapping procedures.

In cases in which multiple acquisitions are not allowable, the last three methods of Table 2, based on a single acquisition, can be taken into account. In particular

1. RGB photoelasticity (without reference fringes) has the advantage of being independent of the isoclinic parameter, although it may give inaccurate results in the range $0 \leqslant \delta \leqslant 0.5$ fringe orders, as previously shown.
2. In the range $0 \leqslant \delta \leqslant 0.5$ fringe orders, the TF method applied by means of RGB photoelasticity

and the ATPM can noticeably mitigate such disadvantage, as previously mentioned.

3. The TF method (applied by means of the CFM) is easy to be applied since the calibration procedure is not required, although the presence of a carrier is needed; this method, where applicable, proves to be very effective.

Declaration of conflicting interests

The authors declare that there is no conflict of interest.

Funding

This research received no specific grant from any funding agency in the public, commercial, or not-for-profit sectors.

References

1. Aben H and Guillemet C. *Photoelasticity of glass*. Berlin: Springer-Verlag, 1993.
2. McKenzie HW and Hand RJ. *Basic optical stress measurement in glass*. Sheffield: Society of Glass Technology, 1999.
3. Redner AS and Voloshin AS. Surface and edge stress in tempered glass. In: *Proceedings of the 9th international conference on experimental mechanics*, vol. 2, Copenhagen, 20–24 August 1990, pp.884–891. Danmarks Tekniske Højskole: Afdelingen for Bærende Konstruktioner.
4. Strainoptics, Inc. 2013, http://www.strainoptics.com
5. ASTM 1279. Standard test method for non-destructive photoelastic measurement of edge and surface stresses in annealed, heat-strengthened, and fully tempered flat glass. In: *Annual book of ASTM standards*. West Conshohocken, PA: ASTM.
6. ASTM C978. Standard test method for photoelastic determination of residual stress in a transparent glass matrix using a polarizing microscope and optical retardation compensation procedures. In: *Annual book of ASTM standards*. West Conshohocken, PA: ASTM.
7. ASTM F218. Standard method for analyzing stress in glass. In: *Annual book of ASTM standards*. West Conshohocken, PA: ASTM.
8. ASTM C148. Standard test method for polariscopic examination of glass containers. In: *Annual book of ASTM standards*. West Conshohocken, PA: ASTM.
9. UNI 7220:1997. *Contenitori di vetro—Rilievo delle tensioni residue*. Milano: UNI (in Italian).
10. Sharples. 2013, http://www.sharplesstress.com
11. Aben H, Anton J and Errapart A. Modern photoelasticity for residual stress measurement in glass. *Strain* 2008; 44: 40–48.
12. GlasStress. 2013, http://www.glasstress.com
13. Ramesh K. *Digital photoelasticity*. Berlin: Springer-Verlag, 2000.
14. Patterson EA. Digital photoelasticity: principles, practice and potential. *Strain* 2002; 38(1): 27–39.
15. Ramesh K, Kasimayan T and Neethi Simon B. Digital photoelasticity—a comprehensive review. *J Strain Anal Eng* 2011; 46: 245–266.
16. Lesniak JR and Zickel MJ. Applications of automated grey-field polariscope. In: *Proceedings of the SEM spring conference on experimental and applied mechanics*, Houston, TX, 1–3 June 1998, pp.298–301. Bethel, CT: Society for Experimental Mechanics.
17. Calvert G, Lesniak JR and Honlet M. Applications of modern automated photoelasticity to industrial problem. *Insight* 2002; 44(2): 224–228.
18. Glass Photonics. 2013, http://www.glassphotonics.com
19. Sanford RJ. On the range of accuracy of spectrally scanned white light photoelasticity. In: *Proceedings of the SEM spring conference on experimental mechanics*, New Orleans, LA, 8–13 June 1986, pp.901–908. Bethel, CT: Society for Experimental Mechanics.
20. Sanford RJ and Iyengar V. The measurement of the complete photoelastic fringe order using a spectral scanner. In: *Proceedings of the SEM conference on experimental mechanics*, Las Vegas, NV, 9–14 June 1985, pp.160–168. Bethel, CT: Society for Experimental Mechanics.
21. Voloshin AS and Redner AS. Automated measurement of birefringence: development and experimental evaluation of the techniques. *Exp Mech* 1989; 29(3): 252–257.
22. Redner A. Automated measurement of edge stress in automotive glass. In: *Proceedings of the conference on glass processing days*, Tampere, 15–18 June 2003, pp.578–599. Tamglass.
23. Ajovalasit A, Petrucci G and Scafidi M. Measurement of edge residual stresses in glass by the phase shifting method. *Opt Laser Eng* 2011; 49(5): 652–657.
24. Aben H, Ainola L and Anton J. Half-fringe phase-stepping with separation of the principal stress directions. *Proc Est Acad Sci: Eng* 1999; 5(3): 198–211.
25. Battaglia S, Ajovalasit A, Petrucci G, et al. Analisi fotoelastica delle tensioni residue nel vetro. *Rivista della Stazione Sperimentale del Vetro* 2010; 40(3): 19–31 (in Italian).
26. Ajovalasit A, Petrucci G and Scafidi M. RGB photoelasticity applied to the analysis of membrane residual stress in glass. *Meas Sci Technol* 2012; 23(2): 025601.
27. Ajovalasit A, Petrucci G and Scafidi M. Analisi delle tensioni residue nel vetro mediante la fotoelasticità con frange di riferimento. In: *Proceedings of the 40th AIAS national congress*, Palermo, 7–10 September 2011 (in Italian). AIAS.
28. Ajovalasit A, Petrucci G and Scafidi M. Photoelastic analysis of edge residual stresses in glass by automated "test fringes" methods. *Exp Mech* 2012; 52(8): 1057–1066.
29. Lavrador MB, Soares ACC, Vieira RD, et al. Automated inspection of residual stresses in glass using RGB photoelasticity. In: *Proceedings of the SEM spring conference on experimental and applied mechanics*, Houston, TX, 1–3 June 1998. Bethel, CT: Society for Experimental Mechanics.
30. Ajovalasit A, Petrucci G and Scafidi M. Photoelastic analysis of edge residual stresses in glass by the automated tint plate method. *Exp Techniques*. Epub ahead of print 19 February 2013. DOI: 10.1111/ext.12017.
31. Haake SJ and Patterson EA. The dispersion of birefringence in photoelastic materials. *Strain* 1993; 29: 3–7.
32. Cloud G. *Optical methods of engineering analysis*. Cambridge, UK: Cambridge University Press, 1995.
33. Ajovalasit A, Petrucci G and Scafidi M. Phase shifting photoelasticity in white light. *Opt Laser Eng* 2007; 45(5): 596–611.
34. Redner AS and Nickola WE. Measurement of residual strains and stresses in transparent materials. *Exp Techniques* 1984; 8(2): 29–32.

35. Haake SJ and Patterson EA. Photoelastic analysis using a full field spectral contents analyser. In: *Proceedings of the SEM conference on experimental mechanics*, Grand Rapids, MI, 12–14 June 1995, pp.342–345. Bethel, CT: Society for Experimental Mechanics.
36. Ivanova L and Nechev G. A method for investigation of the residual stressed in glasses with spectral polariscope. In: *Proceedings of the 9th international conference on experimental mechanics*, Copenhagen, 20–24 August 1990, vol. 2, pp.876–883. Danmarks Tekniske Højskole: Afdelingen for Bærende Konstruktioner.
37. Sanford RJ and McGinnis A. New method for measuring low level birefringence using a spectra scanner. In: *Proceedings of the 37th international instrumentation symposium*, San Diego, CA, 5–9 May 1991, pp.1029–1041. Durham, NC: Instrument Society of America.
38. Ajovalasit A, Barone S and Petrucci G. Toward RGB photoelasticity: full field photoelasticity in white light. *Exp Mech* 1995; 35: 193–200.
39. Ramesh K and Deshmukh SS. Three fringe photoelasticity—use of colour image processing hardware to automate ordering of isochromatics. *Strain* 1996; 32(3): 79–86.
40. Ajovalasit A, Petrucci G and Scafidi M. RGB photoelasticity: review and improvements. *Strain* 2010; 46(2): 137–147.
41. Hecker FW and Morche B. Computer-aided measurement of relative retardations in plane photoelasticity. In: Wieringa H (ed.) *Experimental stress analysis*. Leiden: Martinus Nijhoff Publishers, 1986, pp.535–542.
42. Patterson EA and Wang ZF. Towards full field automated photoelastic analysis of complex components. *Strain* 1991; 27(2): 49–56.
43. Barone S, Burriesci G and Petrucci G. Computer aided photoelasticity by an optimum phase stepping method. *Exp Mech* 2002; 42(2): 132–139.
44. Ajovalasit A, Barone S, Petrucci G, et al. The influence of the quarter wave plates in automated photoelasticity. *Opt Laser Eng* 2002; 38: 31–56.
45. Asundi A. Phase shifting in photoelasticity. *Exp Techniques* 1993; 17: 19–23.
46. Chakrabarti SK and Machin KE. Accuracy of compensation methods in photoelastic fringe-order measurements. *Exp Mech* 1969; 9(8): 429–431.
47. Coelho JM, Silva C and Almeida T. Stress analysis in glass artwork. *Int J Opt* 2011; 2011: 215404 (7 pp.).
48. Madhu KR, Prasath RGR and Ramesh K. Colour adaptation in three fringe photoelasticity. *Exp Mech* 2007; 47(2): 271–276.
49. Kale S and Ramesh K. Advancing front scanning approach for three-fringe photoelasticity. *Opt Laser Eng* 2013; 51(5): 592–599.
50. Quiroga JA, Garcia-Botella A and Gomez-Pedrero JA. Improved method for isochromatic demodulation by RGB calibration. *Appl Optics* 2002; 41(17): 3461–3468.
51. Madhu KR and Ramesh K. Noise removal in three fringe photoelasticity by adaptive colour difference estimation. *Opt Laser Eng* 2007; 45(1): 175–182.
52. Naveen YA, Ramesh K and Ramakrishnan V. Use of carrier fringes in the evaluation of edge residual stresses in a glass plate by photoelasticity. In: *Joint international conference on ISEM-ACEM-SEM-7th ISEM' 2012*, Taipei, paper/J106, http://www.isem2012.tw/full_paper/J106.pdf